Paleoceanography and Paleoclimatology

Supporting Information for

New magnetostratigraphic insights from Iceberg Alley on the rhythms of Antarctic climate during the Plio-Pleistocene

Brendan T. Reilly[1], Lisa Tauxe[1], Stefanie Brachfeld[2], Maureen Raymo[3], Ian Bailey[4], Sidney Hemming[3], Michael E. Weber[5], Trevor Williams[6], Marga Garcia[7], Michelle Guitard[8], Yasmina M. Martos[9, 10], Lara F. Pérez[11], Xufeng Zheng[12], Linda Armbrecht[13], Fabricio G. Cardillo[14], Zhiheng Du[15], Gerson Fauth[16], Anna Glueder[17], Marcus Gutjahr[18], Iván Hernández-Almeida[19], Frida S. Hoem[20], Ji-Hwan Hwang[21], Mutsumi Iizuka[22], Yuji Kato[23], Bridget Kenlee[24], Suzanne O'Connell[25], Victoria Peck[11], Thomas A. Ronge[26], Osamu Seki[27], Shubham Tripathi[28], Jonathan Warnock[29]

[1]Scripps Institution of Oceanography, University of California San Diego, La Jolla, CA 92093, USA
[2]Earth and Environmental Studies, Montclair State University, Montclair, NJ 07043, USA
[3]Lamont-Doherty Earth Observatory, Columbia University, Palisades, NY 10964, USA
[4]Camborne School of Mines and Environmental Sustainability Institute, University of Exeter, Penryn Campus, Cornwall TR10 9FE, UK
[5]Institute for Geosciences, University of Bonn, Bonn 53115, Germany
[6]International Ocean Discovery Program, Texas AM University, College Station, TX 77845, USA
[7]Oceanographic Center of Cadiz, Spanish Institute of Oceanography (IEO), Puerto Pesquero, Muelle de Levante, S/N, Cádiz 11006, Spain
[8]College of Marine Science, University of South Florida, St. Petersburg, FL 33701, USA
[9]Planetary Magnetospheres Laboratory, NASA Goddard Space Flight Center, Greenbelt, MD 20771, USA [10]Department of Astronomy, University of Maryland College Park, College Park, MD 20742, USA
[11]British Antarctic Survey, Cambridge CB3 0ET, UK
[12]South China Sea Institute of Oceanology, Chinese Academy of Sciences, Guangzhou 510301, China
[13]Australian Centre for Ancient DNA, Department of Ecology & Evolutionary Biology, University of Adelaide, South Australia 5005, Australia
[14]Departmento Oceanografia, Servicio de Hidrografia Naval, Ministerio de Defensa, Argentina
[15]State Key Laboratory of Cryospheric Science, Northwest Institute of Eco-Environment and Resources, Chinese Academy of Sciences, Lanzhou 730000, China
[16]Geology Program, University of Vale do Rio dos Sinos, São Leopoldo RS 93022-750, Brazil
[17]College of Earth, Ocean, and Atmospheric Sciences, Oregon State University, Corvallis, OR 97331, USA
[18]GEOMAR Helmholtz Centre for Ocean Research Kiel, 24148 Kiel, Germany
[19]Department of Earth Sciences, ETH Zürich, 8092 Zurich, Switzerland
[20]Department of Earth Sciences, Marine Palynology and Paleoceanography, Utrecht University, 3584 CB Utrecht, Netherlands

[21]Earth Environmental Sciences, Korea Basic Science Institute, Chungbuk Cheongju, Republic of Korea
[22]Knowledge Engineering, Tokyo City University, Tokyo setagaya-ku 158-0087, Japan
[23]Center for Advanced Marine Core Research, Kochi University, Monobe, Nankoku, Kochi 783-8502, Japan
[24]Department of Earth Sciences, University of California Riverside, Riverside, CA 92521, USA
[25]Department of Earth and Environmental Sciences, Wesleyan University, Middletown, CT 06459, USA
[26]Alfred Wegener Institute, Helmholtz Center for Polar and Marine Research, 27568 Bremerhaven, Germany
[27]Institute of Low Temperature Science, Hokkaido University, Sapporo Hokkaido 060-0819, Japan
[28]Marine Stable Isotope Lab, National Centre for Polar and Ocean Research, Ministry of Earth Sciences, Vasco Da Gama 403804, India
[29]Department of Geoscience, Indiana University of Pennsylvania, Indiana, PA 15705, USA

Corresponding author: Brendan T. Reilly, btreilly@ucsd.edu

Contents of this file

Figures S1 to S4

Additional Supporting Information (Files uploaded separately)

Captions for Tables S1 to S14

Introduction

Supporting information include 4 supplementary figures and 14 supplementary tables. Supplementary tables are included as a separate Excel file, with each table as a sperate sheet.

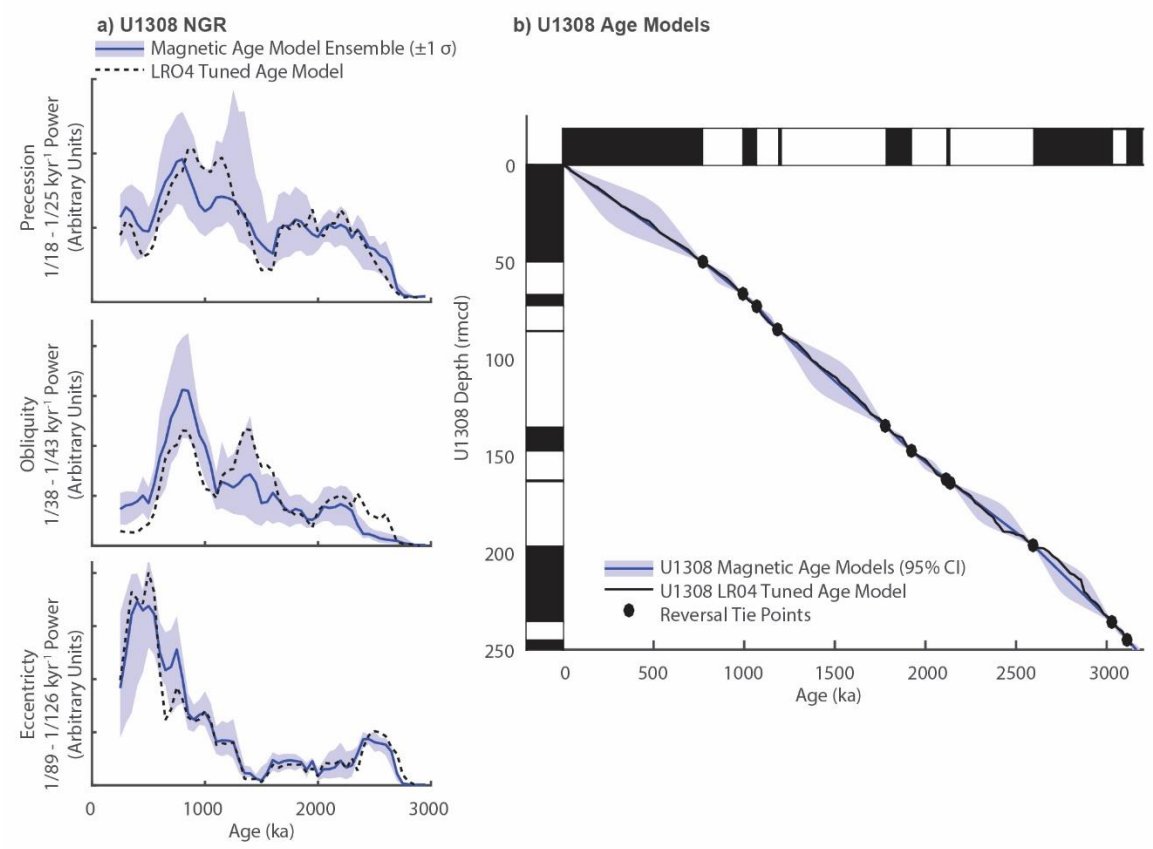

Figure S1. (a) Comparison of the spectral power of the IODP Site U1308 NGR record in frequency bands associated with eccentricity, obliquity, and precession of an ensemble of magnetic reversal constrained age models (blue line = median power; blue shading = ±1σ) and the LR04 (Lisiecki & Raymo, 2005) tuned benthic $\delta^{18}O$ age model (black dashed line) (Channell et al., 2016; Hodell & Channell, 2016). Analysis is the same as and can be compared to the Dove Basin results plotted in Figure 7 of the main text. **(b)** Comparison of the IODP Site U1308 LR04 tuned age model (black line) and the ensemble of magnetic reversal age models (median = blue line; 95% interval = blue shading) generated using Undatable (Lougheed & Obrochta, 2019). The magnetic reversal age models were generated in the same fashion as those generated for Dove Basin and can be compared to the results plotted in Figure 5 of the main text.

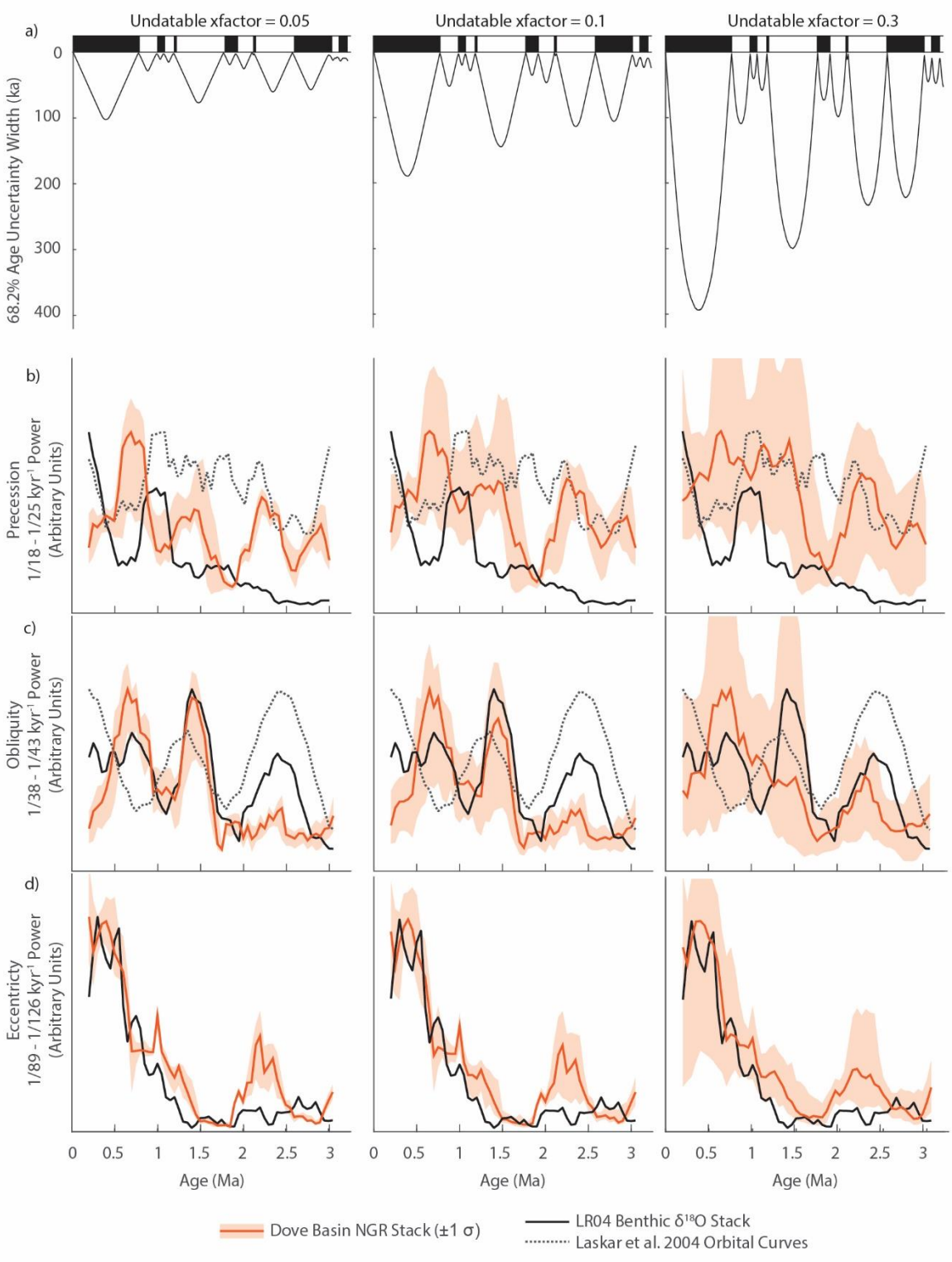

Figure S2. Comparison of the spectral power of the Dove Basin NGR stack on age models constructed using three different Undatable *xfactors* that Lougheed and Obrochta (2019) consider realistic, 0.05, 0.1, and 0.3. Note that the results presented and discussed in the main text (Figure 7) use an *xfactor* of 0.1. **(a)** Comparison of the width of the 68.2% age model

uncertainty calculated at each *xfactor* and the geomagnetic polarity timescale (black = normal; white = reverse). **(b-d)** Spectral power of the Dove Basin NGR stack (scaled to maximum value) of the Dove Basin NGR stack (orange line = median; orange shading shading = ±1 sigma range from the ensembles of magnetostratigraphic age models calculated using three different *xfactors*), the LR04 benthic $\delta^{18}O$ stack (solid black line; Lisiecki & Raymo, 2005), and the Laskar et al. orbital parameters (2004; dashed line) for **(b)** climatic precession and **(c)** obliquity angle. **(b)** Power in frequencies associated with Earth's precession (1/18 – 1/25 kyr^{-1}), **(c)** power in the frequency associated with Earth's obliquity (1/38 – 1/43 kyr^{-1}), and **(d)** power in the frequency associated with Earth's eccentricity (1/89 – 1/126 kyr^{-1}).

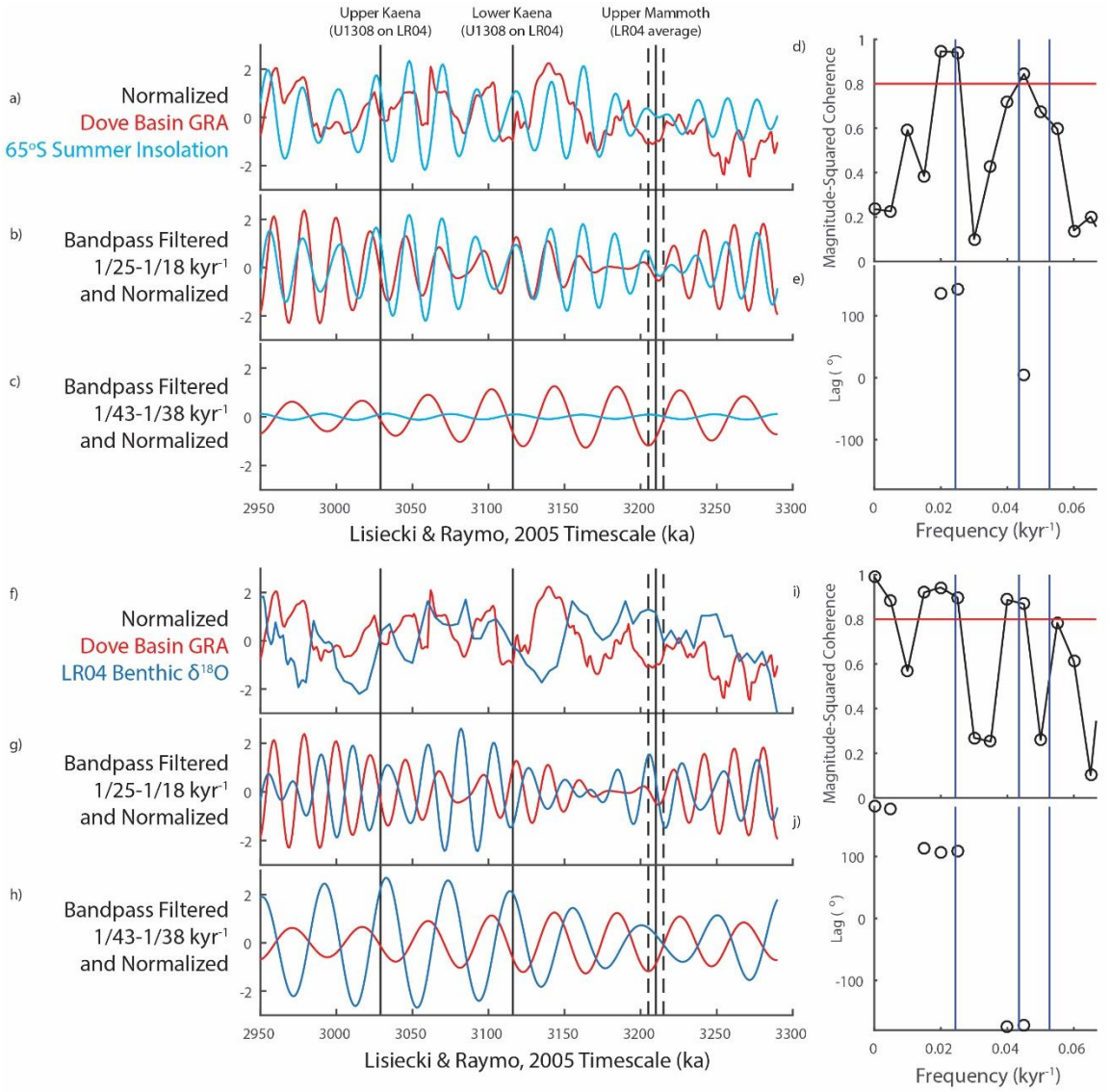

Figure S3. Comparing the late Pliocene Dove Basin gamma ray attenuation (GRA) stack (red) with **(a-c)** 65^0 S summer insolation (light blue; Laskar et al., 2004) and the **(f-h)** LR04 benthic $\delta^{18}O$ stack (dark blue; Lisiecki & Raymo, 2005). A bandpass filter is used to visualize variation in the frequencies associated with **(b and g)** precession (1/25-1/18 kyr^{-1}) and **(c and h)** obliquity (1/43-1/38 ky^{-1}) paced variations. Bandpass filtered data are normalized by the standard deviation of the 1/25-1/18 kyr^{-1} filtered data for each record so that relative amplitudes can be compared. **(d and i)** Coherence and **(e and j)** phase for frequency bands, with phase plotted only for frequencies with magnitude squared coherence greater than 0.8. The Dove Basin GRA record is in phase (~0 kyr lag) with 65^0 S summer insolation and out-of-phase with LR04 benthic $\delta^{18}O$ (~12 kyr lag) in the frequencies associated with precession paced variations. The Dove Basin GRA record lags 65^0 S summer insolation (~16 kyr lag) and LR04 benthic $\delta^{18}O$ (~12 kyr lag) in the frequencies associated with obliquity paced variations. Note that the phase analysis is performed on the LR04 timescale and could reflect LR04 timescale uncertainties discussed in the main text, particularly for the comparison to insolation.

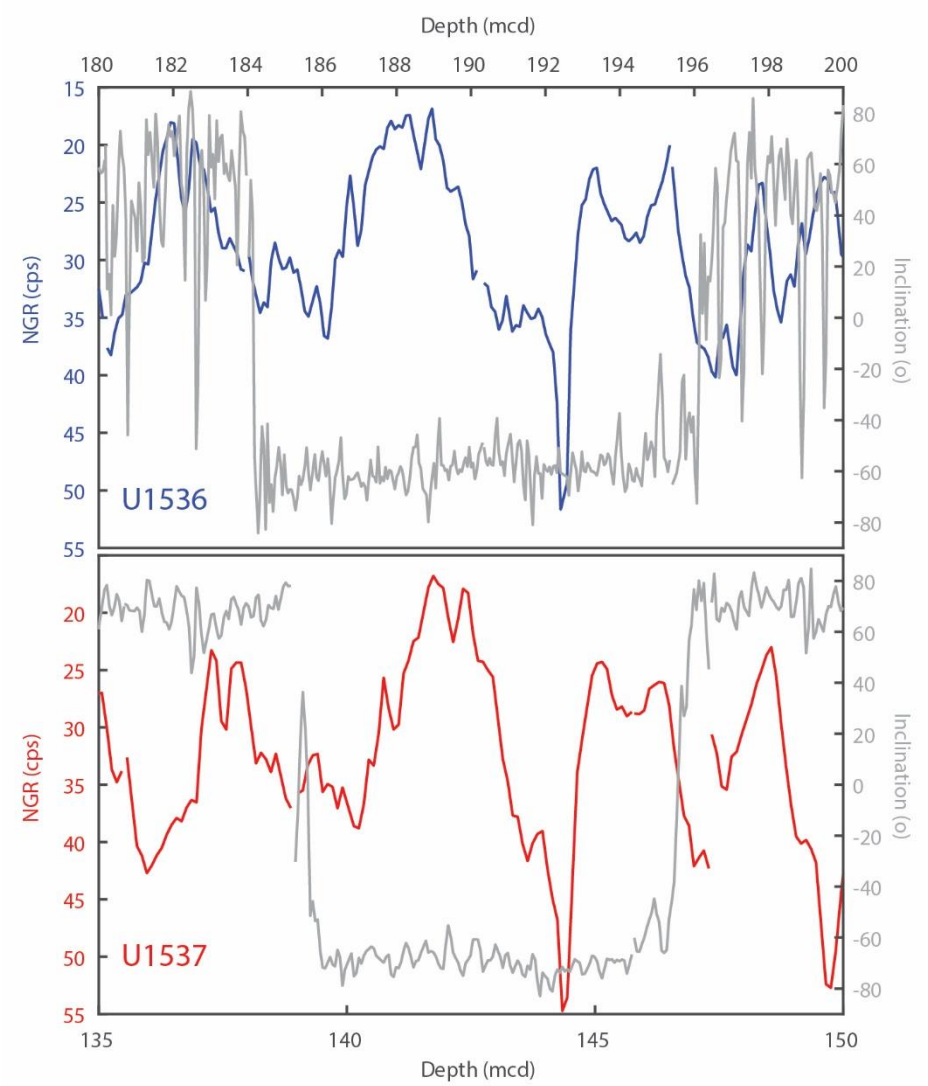

Figure S4. Natural Gamma Radiation (NGR) and Inclination after 15 mT alternating field demagnetization at IODP Sites U1536 (blue) and U1537 (red) around the C1r.1n (Jaramillo) Subchron. Note while the U1536 inclination record is noisier, the positions of the magnetic reversals are consistent relative to NGR at the two sites.

Table S1. Splice table and additional appended cores for Site U1536 used in this study.

Table S2. Splice table and additional appended cores for Site U1537 used in this study.

Table S3. Correlation table for creation of correlated equivalent depth (ced) scale between Sites U1536 and U1537.

Table S4. Uncertainty estimates for Site U1536 natural gamma radiation (NGR) correlation to Site U1537 on mcd depth scale using Undatable (Lougheed & Obrochta, 2019).

Table S5. Site U1536 inclination, natural gamma radiation (NGR), gamma ray attenuation (GRA), and b* data used in this study.

Table S6. Site U1537 inclination, natural gamma radiation (NGR), gamma ray attenuation (GRA), and b* data used in this study.

Table S7. Meters below sea floor (mbsf) depths of magnetic reversals at Site U1536. Reversal ages are those used in this study's age models (see Methods; Channell et al., 2016; Lisiecki & Raymo, 2005).

Table S8. Meters composite depth (mcd) splice depths of magnetic reversals at Site U1536. Reversal ages are those used in this study's age models (see Methods; Channell et al., 2016; Lisiecki & Raymo, 2005).

Table S9. Meters below sea floor (mbsf) depths of magnetic reversals at Site U1537. Reversal ages are those used in this study's age models (see Methods; Channell et al., 2016; Lisiecki & Raymo, 2005).

Table S10. Meters composite depth (mcd) splice depths of magnetic reversals at Site U1537. Reversal ages are those used in this study's age models (see Methods; Channell et al., 2016; Lisiecki & Raymo, 2005).

Table S11. Magnetostratigraphic age model for Site U1536 generated with Undatable (Lougheed & Obrochta, 2019).

Table S12. Magnetostratigraphic age model for Site U1537 generated with Undatable (Lougheed & Obrochta, 2019).

Table S13. Dove Bain data stacks used in this study.

Table S14. Stratigraphic summary of magnetic reversals discussed in this study. U1308 ages from Channell et al., (2016). In relation to benthic $\delta^{18}O$, warm intervals are intervals with more positive values. In relation to Dove Basin facies, warm intervals are intervals with high higher b*, lower NGR, and lower GRA.

References

Channell, J. E. T., Hodell, D. A., & Curtis, J. H. (2016). Relative paleointensity (RPI) and oxygen isotope stratigraphy at IODP Site U1308: North Atlantic RPI stack for 1.2–2.2 Ma (NARPI-2200) and age of the Olduvai Subchron. *Quaternary Science Reviews*, *131*, 1–19. https://doi.org/10.1016/j.quascirev.2015.10.011

Hodell, D. A., & Channell, J. E. (2016). Mode transitions in Northern Hemisphere glaciation: co-evolution of millennial and orbital variability in Quaternary climate. *Climate of the Past*, *12*(9), 1805.

Laskar, J., Robutel, P., Joutel, F., Gastineau, M., Correia, A. C. M., & Levrard, B. (2004). A long-term numerical solution for the insolation quantities of the Earth. *Astronomy & Astrophysics*, *428*(1), 261–285. https://doi.org/10.1051/0004-6361:20041335

Lisiecki, L. E., & Raymo, M. E. (2005). A Pliocene-Pleistocene stack of 57 globally distributed benthic $\delta^{18}O$ records. *Paleoceanography*, *20*(1), PA1003. https://doi.org/10.1029/2004PA001071

Lougheed, B., & Obrochta, S. (2019). A Rapid, Deterministic Age-Depth Modeling Routine for Geological Sequences With Inherent Depth Uncertainty. *Paleoceanography and Paleoclimatology*, *0*(0). https://doi.org/10.1029/2018PA003457